

Atomic and electronic structures of Pd₁₃ and Pt₁₃ clusters

Noriko Watari

NEC Informatec Systems, Ltd., KSP R&D Building, Sakato 3-2-1, Takatsu-ku, Kawasaki, Kanagawa 213, Japan

Shuhei Ohnishi

NEC Fundamental Research Laboratory, Miyukigaoka 34, Tsukuba, Ibaraki 305, Japan

(Received 20 June 1997; revised manuscript received 9 February 1998)

The electronic structures of Pd₁₃ and Pt₁₃ clusters of cuboctahedral and icosahedral symmetries are analyzed by the self-consistent spin-polarized density-functional scheme using the norm-conserving pseudopotential in the linear combination of atomic orbitals method. The electronic structure is discussed in relation to the shell structure of the giant atom. The stable atomic structure is discussed, considering the effects of the generalized gradient approximation of the exchange-correlation potential, the spin-orbit splitting, and the Jahn-Teller effect. The spin-orbit coupling effect depends on the symmetry of the whole cluster. It is the largest of these effects for Pt, and it is as large as the spin polarization effect for Pd. The electronic structure of Pd and Pt clusters of 13 atoms is comprehended as a complex of the shell structure and the localized Pd-4*d* or Pt-5*d* orbitals. The Jahn-Teller effect seems to be small to keep the shell structure. For both Pd and Pt metals the cuboctahedron clusters are more stable and have small spin polarization, $S=3$ for the Pd cluster and $S=4$ for the Pt cluster. [S0163-1829(98)02527-2]

I. INTRODUCTION

The spin configuration of a microcluster is important to determine the stable structure of an isomer or its magnetism. Reddy *et al.* reported that 13-atom clusters of 3*d* and 4*d* metals, especially in the icosahedral symmetry, have nonzero magnetic moments,^{1,2} and this is why the icosahedron structure is the most stable for Pd₁₃, Rh₁₃, Ru₁₃, and Fe₁₃. Recently the magnetism of the Pd cluster was discussed intensively and suspected to have no magnetic moment.³ Zhao *et al.* have shown that the magnetic-nonmagnetic transition in nonmagnetic 3*d* and 4*d* metal clusters is roughly estimated by a simple analytic equation based on a tight-binding Friedel model⁴ and this generally agrees with recent experimental results.⁵⁻⁷ The magnetism emerges when the cluster size becomes smaller and the critical size for Pd calculated by Zhao's scheme is 8. The magnetic moment for Pd₁₃ calculated by Reddy *et al.* is $0.43\mu_B/\text{atom}$,² which is consistent with the experimental upper bound of $<0.40\mu_B/\text{atom}$ ⁶ palladium clusters being essentially nonmagnetic.

Our previous calculation on Pt₁₃ clusters using the spin restricted approximation proposed that the cuboctahedron cluster was the most stable within that approximation, but the state was not a closed shell.⁸ Noble metal clusters of 13 atoms, which have one delocalized valence electron and a closed atomic *d*-shell per atom, are understood as a shell structure of *s*-electrons that is interacting with the atomic *d*-electron-band.^{9,11} The shell structure of transition-metal clusters was also investigated for Ni clusters with discrete-variational $X\alpha$ (DV- $X\alpha$) by Fujima *et al.*¹⁰ and for Pt with a pseudopotential by Watari and Ohnishi.⁸ Fujima's group analyzed the shell structure apart from the atomic *d*-band and labeled 1*s*, 1*p*, 1*d*, . . . shells across the atomic *d*-band. We concluded that the shell structure also exists in the atomic *d*-band, the $n=1$ shell terminates there, and that it is appropriate to label the one above the atomic *d*-band as the n

$=2$ shell, which explains well the structure of the cluster with adsorbed hydrogen.

Microclusters of Pd and Pt are also important as industrial catalysts. They are used for various oxidation, hydrogenation, and dehydrogenation reactions involving hydrocarbons.¹² It is known that the catalytic activity may often be improved by adding small amounts of alkali metals. The mechanism of these catalytic processes is not understood theoretically. It may be related to the fundamental properties of microclusters.

In this paper we address the discussion of the interrelation between the shell structure and the spin configuration, the effect of the generalized gradient approximation (GGA) for the exchange-correlation potential, the effect of spin-orbit interaction, and the Jahn-Teller effect. Section II describes our method. Section III presents the results of total energy analysis of the different spin configurations of the Pd and Pt clusters of the 13-atom icosahedron and cuboctahedron, the shell structure analysis, the spin-orbit interaction analysis, and the effect of Jahn-Teller distortion. Section IV discusses these results in general.

II. CALCULATION METHOD

The linear combination of norm-conserving pseudopotential atomic orbitals (LCPSAO) method is characterized by introducing the well known effective core potential,¹³ and the nodeless radial wave function, which are determined by the self-consistent solution of the Dirac equation for a single atom. Details of the calculation scheme are described in our previous papers.^{8,11,14,15}

The total Hamiltonian for the present system is written as

$$H_\sigma = \left[-\frac{1}{2} \nabla^2 + \sum_{it} \hat{V}_{it}^{ps}(\mathbf{r} - \mathbf{R}_i) + V_{\text{val}}^\sigma(\mathbf{r}) \right], \quad (1)$$

TABLE I. Summary of spin restricted results (LDA).

Cluster (sym.)	Equilibrium spacing (a.u.)	Total energy (Hartree)	HOMO		LUMO		HOMO-LUMO gap (Hartree)
			sym.	energy	sym.	energy	
Pd ₁₃ fcc (<i>O_h</i>)	5.1	-376.578	<i>e_g</i> (4)	-0.2129	<i>t_{1u}</i>	-0.207 64	0.005 26
Pd ₁₃ fcc (<i>D_{3d}</i>)	5.1	-376.580					
Pd ₁₃ icos (<i>I_h</i>)	5.1	-376.531	<i>t_{2g}</i> (4)	-0.208 73	<i>t_{1u}</i>	-0.207 72	0.001 01
Pd ₁₃ icos (<i>D_{3d}</i>)	5.1	-376.529					
Pt ₁₃ fcc (<i>O_h</i>)	5.1	-341.802	<i>t_{1g}</i> (2)	-0.215 89	<i>a_{2g}</i>	-0.214 40	0.001 49
Pt ₁₃ fcc (<i>D_{3d}</i>)	5.1	-341.801					
Pt ₁₃ icos (<i>I_h</i>)	5.0	-341.751	<i>t_{1g}</i> (4)	-0.217 77	<i>t_{2g}</i>	-0.207 90	0.009 87
Pt ₁₃ icos (<i>D_{3d}</i>)	5.0	-341.751					

$$H_{\sigma}\psi_{\nu}^{\sigma} = \varepsilon_{\nu}^{\sigma}\psi_{\nu}^{\sigma}, \quad (2)$$

where \mathbf{R}_i is the atomic site i . \hat{V}_{il}^{ps} is the effective core pseudopotential for the atom located at the site \mathbf{R}_i , which is given by the sum of the long-range core potential $V_{\text{core}}(\mathbf{r})$ and the nonlocal angular-momentum-dependent potential $\hat{V}_l^{\text{ion}}(\mathbf{r})$.¹³ V_{val}^{σ} is the sum of Coulomb potential V_C and the exchange-correlation potential V_{XC}^{σ} given by $V_{\text{XC}}^{\sigma}(\mathbf{r}) = \partial E_{\text{XC}} / \partial \rho_{\sigma}(\mathbf{r})$, where $E_{\text{XC}}[\rho, s]$ is the exchange-correlation energy. ψ_{ν}^{σ} and $\varepsilon_{\nu}^{\sigma}$ are the wave function and the eigenvalue of the state ν and spin σ . $\rho(\mathbf{r})$ is the electron density. We use the spin-polarized exchange-correlation energy given by Perdew and Zunger,¹⁶ and the generalized gradient approximation (GGA) of the Perdew-Burke-Ernzerhof (PBE) formula as the GGA functional.¹⁷

The nodeless feature of atomic radial wave functions made it feasible to perform numerical integrations for overlap and Hamiltonian matrix elements in the standard LCAO scheme. Multicenter numerical integration is transformed to a single-center one by applying Becke's algorithm.¹⁸

The variational basis functions of this Hamiltonian are atomic orbitals $\chi_{lm}(|\mathbf{r}|) = \phi_l(|\mathbf{r}|)Y_{lm}(\theta, \varphi)$, which are given by solving the *Schrödinger* equation for the norm-conserving pseudopotential self-consistently. The molecular orbital ψ_{ν} represented by the linear combination of symmetrized orbitals is determined by the standard density-functional scheme. The total energy is given by

$$E_{\text{tot}} = \sum_{\nu, \sigma} f_{\nu}^{\sigma} \varepsilon_{\nu}^{\sigma} - \frac{1}{2} \int \int \frac{\rho(\mathbf{r})\rho(\mathbf{r}')}{|\mathbf{r} - \mathbf{r}'|} d\mathbf{r}d\mathbf{r}' + E_{\text{XC}} - \sum_{\sigma} \int \rho_{\sigma}(\mathbf{r}) V_{\text{XC}}^{\sigma}(\rho(\mathbf{r}), s) d\mathbf{r} + \sum_{i < j} \frac{Z_i Z_j}{|\mathbf{R}_i - \mathbf{R}_j|}, \quad (3)$$

where f_{ν}^{σ} is the occupation number at the eigenstate ν for σ spin state.

The Coulomb energy requires the highest accuracy in determining the total energy of the cluster. In the LCPSAO method, the Coulomb potential is calculated by the sum of the potential of each atomic site due to the charge density projected onto spherical harmonics with $l=0, \dots, 8$.

In this work we used a cuboctahedron and an icosahedron for 13-atom clusters.

III. RESULTS

A. Summary of spin restricted results

The equilibrium cluster size, the total energy, and the HOMO-LUMO orbitals of Pd₁₃ and Pt₁₃ clusters obtained by the spin restricted calculation are summarized in Table I. The cluster size is denoted by the distance between the center atom and a peripheral atom. The distance between the peripheral atoms is equal to that between the center atom and a peripheral atom in the cuboctahedron cluster, but in the icosahedron cluster the distance between the peripheral atoms is 5% longer than that between the center atom and a peripheral atom. The experimental nearest-neighbor distances of the bulk are 5.198 a.u. for Pd and 5.242 a.u. for Pt. The distances between the center atom and a peripheral atom are 2% smaller in Pd clusters, 3% smaller in the Pt cuboctahedron cluster, and 5% smaller in the Pt icosahedron cluster. The interatomic distances in microclusters generally shrink. The HOMO's are not closed orbitals except for the Pd₁₃ cuboctahedron cluster and so spin unrestricted calculations are needed. The LUMO's of both Pd clusters are the shell-2*p* states of a big atom, which we describe in detail in the following subsections. To check the effect of the symmetrized orbital, the common symmetry subgroup for *O_h* and *I_h*, *D_{3d}* is also used for the total energy calculation at the equilibrium spacing. The difference using the symmetrized orbital is about 0.002 Hartree.

Table II shows the results with the GGA potential. The changes in the total energy are about -0.01 Hartree for the Pd₁₃ clusters and about -0.001 Hartree for the Pt₁₃ clusters. The equilibrium spacing of the Pd₁₃ icosahedron cluster is slightly (2%) shrunk. The electronic structures are unchanged.

B. Pd₁₃ clusters

1. The Pd₁₃ cuboctahedron cluster

By specifying the number of unpaired electrons of the system and scaling the cluster size by the distance between the center atom and a peripheral atom, we have determined the self-consistent total energy. The total spin is polarized until the total energy becomes higher than that of the system with one less total spin. The spin configurations around the Fermi level and the total energies by LSDA are summarized in Table III. The system with $S=0$ has a closed orbital struc-

TABLE II. Summary of spin restricted results (GGA).

Cluster (sym.)	Equilibrium spacing (a.u.)	Total energy (Hartree)	HOMO		LUMO		HOMO-LUMO gap (Hartree)
			sym.	energy	sym.	energy	
Pd ₁₃ fcc (<i>O_h</i>)	5.1	-376.588	<i>e_g</i> (4)	-0.214 09	<i>t_{1u}</i>	-0.209 24	0.004 85
Pd ₁₃ icos (<i>I_h</i>)	5.0	-376.540	<i>t_{2g}</i> (4)	-0.210 86	<i>t_{1u}</i>	-0.210 41	0.000 45
Pt ₁₃ fcc (<i>O_h</i>)	5.1	-341.803	<i>t_{1g}</i> (2)	-0.215 94	<i>a_{2g}</i>	-0.214 46	0.001 48
Pt ₁₃ icos (<i>I_h</i>)	5.0	-341.752	<i>t_{1g}</i> (4)	-0.217 89	<i>t_{2g}</i>	-0.208 01	0.009 88

ture and the most stable total energy and the energy gap for other systems is on the order of 0.001 Hartree (0.03 eV). Our result agrees with the report by Reddy *et al.*² that the Pd₁₃ cuboctahedron cluster has no magnetic moment by their LDF solution.

Table IV summarizes the results with the GGA potential. The basic electronic structure is not altered. The energies of the systems that have larger spin-polarization are more stable with the GGA potential, which is the most prominent difference from the results with LSDA potential.

We have also analyzed the shell structure by the one-center spherical harmonics expansion of the density of states (DOS) using the following scheme:⁸

$$\tilde{\psi}_{vlm}^{j,\sigma}(r') = \int \psi_v^\sigma(\mathbf{r}) Y_{lm}(\mathbf{r}_j) d\Omega_j, \quad (4)$$

TABLE III. Spin configuration around Fermi level and total energy of Pd₁₃ cuboctahedron cluster by LSDA. ΔE is the difference of total energy from the spin restricted result.

S	Spacing (a.u.)	Spin configuration				ΔE (Hartree)
		Majority-spin		Minority-spin		
0	5.1	<i>t_{1u}</i> (shell-2 <i>p</i> [*])	0	<i>t_{1u}</i> (shell-2 <i>p</i> [*])	0	0.0
		<i>e_g</i>	2	<i>e_g</i>	2	
		<i>a_{2g}</i>	1	<i>a_{2g}</i>	1	
		<i>t_{2g}</i>	3	<i>t_{2g}</i>	3	
1	5.1	<i>a_{1u}</i>	0	<i>a_{1u}</i>	0	+0.004
		<i>t_{1u}</i> (shell-2 <i>p</i> [*])	1	<i>t_{1u}</i> (shell-2 <i>p</i> [*])	0	
		<i>t_{2g}</i>	3	<i>t_{2g}</i>	2	
		<i>e_g</i>	2	<i>e_g</i>	2	
		<i>t_{1g}</i>	3	<i>t_{1g}</i>	3	
		<i>a_{2g}</i>	1	<i>a_{2g}</i>	1	
2	5.1	<i>a_{1u}</i>	0	<i>a_{1u}</i>	0	+0.001
		<i>t_{1u}</i> (shell-2 <i>p</i> [*])	2	<i>t_{1u}</i> (shell-2 <i>p</i> [*])	0	
		<i>t_{1g}</i>	3	<i>t_{1g}</i>	1	
		<i>a_{2g}</i>	1	<i>a_{2g}</i>	1	
		<i>t_{2g}</i>	3	<i>t_{2g}</i>	3	
		<i>e_g</i>	2	<i>e_g</i>	2	
3	5.0	<i>a_{1u}</i>	0	<i>a_{1u}</i>	0	+0.013
		<i>t_{1u}</i> (shell-2 <i>p</i> [*])	3	<i>t_{1u}</i> (shell-2 <i>p</i> [*])	0	
		<i>t_{1g}</i>	3	<i>t_{1g}</i>	0	
		<i>t_{2g}</i>	3	<i>t_{2g}</i>	3	
		<i>e_g</i>	2	<i>e_g</i>	2	
		<i>a_{2g}</i>	1	<i>a_{2g}</i>	1	

$$\varrho_{vlm}^{j,\sigma} = \int (\tilde{\psi}_{vlm}^{j,\sigma}(r_j))^2 r_j^2 dr_j, \quad (5)$$

$$r_j = |\mathbf{r} - \mathbf{R}_j|, \quad (6)$$

$$r_j \leq R_{\max}, \quad (7)$$

TABLE IV. Spin configuration around Fermi level and total energy of Pd₁₃ cuboctahedron cluster with GGA. ΔE is the difference of total energy from the spin restricted result of GGA at $R = 5.1$.

S	Spacing (a.u.)	Spin configuration				ΔE (Hartree)
		Majority-spin		Minority-spin		
0	5.1	<i>t_{1u}</i> (shell-2 <i>p</i> [*])	0	<i>t_{1u}</i> (shell-2 <i>p</i> [*])	0	0.0
		<i>e_g</i>	2	<i>e_g</i>	2	
		<i>t_{2g}</i>	3	<i>t_{2g}</i>	3	
		<i>a_{2g}</i>	1	<i>a_{2g}</i>	1	
1	5.1	<i>a_{1u}</i>	0	<i>a_{1u}</i>	0	-0.001
		<i>t_{1u}</i> (shell-2 <i>p</i> [*])	1	<i>t_{1u}</i> (shell-2 <i>p</i> [*])	0	
		<i>t_{1g}</i>	3	<i>t_{1g}</i>	2	
		<i>e_g</i>	2	<i>e_g</i>	2	
		<i>t_{2g}</i>	3	<i>t_{2g}</i>	3	
		<i>a_{2g}</i>	1	<i>a_{2g}</i>	1	
2	5.1	<i>a_{1u}</i>	0	<i>a_{1u}</i>	0	-0.004
		<i>t_{1u}</i> (shell-2 <i>p</i> [*])	2	<i>t_{1u}</i> (shell-2 <i>p</i> [*])	0	
		<i>t_{1g}</i>	3	<i>t_{1g}</i>	1	
		<i>a_{2g}</i>	1	<i>a_{2g}</i>	1	
		<i>e_g</i>	2	<i>e_g</i>	2	
		<i>t_{2g}</i>	3	<i>t_{2g}</i>	3	
3	5.1	<i>a_{1u}</i>	0	<i>a_{1u}</i>	0	-0.015
		<i>t_{1u}</i> (shell-2 <i>p</i> [*])	3	<i>t_{1u}</i> (shell-2 <i>p</i> [*])	0	
		<i>t_{1g}</i>	3	<i>t_{1g}</i>	0	
		<i>a_{2g}</i>	1	<i>a_{2g}</i>	1	
		<i>t_{2g}</i>	3	<i>t_{2g}</i>	3	
		<i>e_g</i>	2	<i>e_g</i>	2	
4	5.1	<i>a_{1u}</i>	1	<i>a_{1u}</i>	0	-0.008
		<i>t_{1u}</i> (shell-2 <i>p</i> [*])	3	<i>t_{1u}</i> (shell-2 <i>p</i> [*])	0	
		<i>t_{1g}</i>	3	<i>t_{1g}</i>	0	
		<i>a_{2g}</i>	1	<i>a_{2g}</i>	0	
		<i>t_{2g}</i>	3	<i>t_{2g}</i>	3	
		<i>e_g</i>	2	<i>e_g</i>	2	

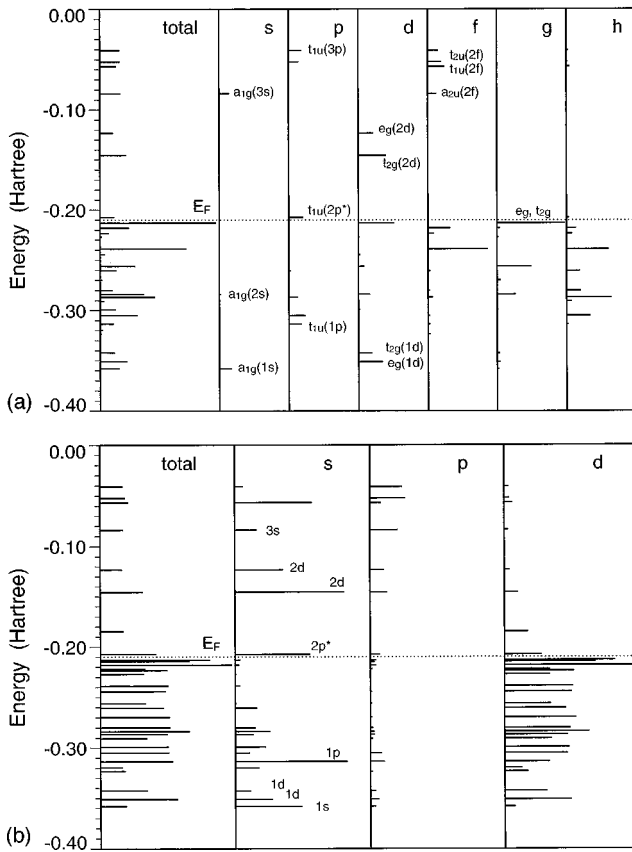


FIG. 1. (a) Energy levels and the density of states (DOS) of Pd_{13} cuboctahedron cluster. s , p , d , f , g , and h indicate the partial DOS of each molecular orbital projected at the cluster center. R_{max} for expansion is 15 Å. (b) Same as (a) but augmented at 13 Pd atom sites with $R_{\text{max}}=1.6$ Å.

where ρ_{ν}^{σ} is the molecular orbital density of state ν of spin σ . Figure 1(a) shows energy levels and the DOS of the Pd_{13} cuboctahedron cluster. s , p , d , f , g , and h indicate the partial DOS, $\rho_{\nu lm}^{\sigma}$, of each molecular orbital projected at the cluster center with $R_{\text{max}}=15$ Å. Comparing with the jellium shell model,¹⁹ these states can be identified with the shell structure. The electronic structure of a d -metal cluster could be understood as a complex system of the shell structure and the atomic d -band.^{9,10,8} The orbital components can be seen by Fig. 1(b), where the DOS is projected at each Pd site with $R_{\text{max}}=1.6$ Å and accumulated for 13 Pd atoms. To compare the orbital components by the coefficient of the atomic orbital, $\rho_{\nu lm}^{\sigma}$ is divided by the degeneracy of the angular momentum l . The states whose atomic s -orbital coefficient is larger than the atomic d -orbital one are thought to construct the skeleton of the shell structure.

The d -electron band is located in the energy range of -0.33 to -0.21 Hartree, which is almost the entire region below the Fermi level. The lowest level, denoted as a_{1g} , in Fig. 1(a) corresponds to the $1s$ level of the shell structure; the next two, e_g and t_{2g} of relatively large s -component, are the shell- $1d$ levels; and the t_{1u} state at about -0.33 Hartree, the edge of the atomic d -band, is the shell- $1p$ level. The inversion of the shell- $1p$ and $-1d$ states is caused by the interaction between the shell- $1d$ and the atomic d -band. The interaction of the shell- $1p$ with the d -band seems to be

smaller than that of the shell- $1d$, for the s -coefficient ratio of the shell- $1p$ is larger than that of the shell- $1d$ and the position of the shell- $1p$ is the edge of the atomic d -band. The t_{1u} state just above the Fermi level whose s -component is extremely large is the shell- $2p^*$ state. The total energy becomes higher when the shell- $2p^*$ state is occupied in the LSD approximation but this does not hold for GGA. The higher spin state of GGA is stabler than the closed orbital structure. The HOMO corresponds to the shell- $1g$, which is shown in Fig. 1.

2. The Pd_{13} icosahedron cluster

The icosahedron cluster of the Pd_{13} is analyzed in the same way as the Pd_{13} cuboctahedron cluster. The spin configurations around the Fermi level and the total energies are summarized in Table V. The results of both LSDA and GGA potentials are listed together because there is no prominent difference. The system of $S=4$ is the most stable in the Pd_{13} icosahedron cluster, whose total energy is similar to the $S=3$ system of the Pd_{13} cuboctahedron cluster. The cuboctahedron cluster is more stable than the icosahedron cluster in Pd_{13} clusters.

The shell structure of the $S=4$ system is shown in Fig. 2(a), and the components of each level are shown in Fig. 2(b). The atomic d -electron band is located in the energy range of about -0.33 to -0.22 Hartree for the majority spin and about -0.32 to -0.20 Hartree for minority spin. The atomic d -band is further divided into two regions from the point of view of the blending of the atomic s -orbital. In the region lower than -0.28 Hartree, the atomic s -component is rather large. The lowest level denoted as a_{1g} in Fig. 2(a) corresponds to the $1s$ level of the shell structure, which is almost degenerate with the next level of h_g in the majority spin. The t_{1u} state at about -0.33 to -0.32 Hartree of the edge of the atomic d -band is the shell- $1p$ level. The reason for the inversion of the shell- $1p$ and $-1d$ states is the same as that for the cuboctahedron cluster: the interaction between the shell- $1d$ with the atomic d -band. The t_{1u} states just above the Fermi level in the majority spin and just below the Fermi level in the minority spin whose s -component is extremely large are the shell- $2p^*$ states. The energy levels in the atomic d -band, which have comparatively large atomic s -component, can be regarded as the shell states. Those are labeled in Figs. 2(a) and 2(b).

In the icosahedron cluster, the $S=0$ system does not have a closed orbital, unlike that of the cuboctahedron cluster. The t_{1u} state corresponding to the shell- $2p^*$ is occupied in the majority spin of the Pd_{13} icosahedron cluster. The total energy becomes higher when the h_g state of the shell- $2d$ is occupied, which corresponds to the $S=5$ system. The gap in total energy between the cuboctahedron and icosahedron clusters is about 0.05 Hartree with both LDA and GGA potential.

C. Pt_{13} clusters

1. The Pt_{13} cuboctahedron cluster

By varying the number of unpaired electrons and the cluster spacing, we calculate the total energy. The equilibrium distance of the Pt_{13} cuboctahedron cluster is 5.1 a.u., which

TABLE V. Spin configuration around Fermi level and total energy of Pd₁₃ icosahedron cluster. ΔE is the difference of total energy from the spin restricted result of LSDA. Superscript ‘‘g’’ represents a value at equilibrium spacing of GGA. The other values are calculated at equilibrium spacing of LSDA.

S	Spacing (a.u.)	Spin configuration		ΔE by LSDA (Hartree)	ΔE by GGA (Hartree)	
		Majority-spin	Minority-spin			
0	5.1	h_g (shell-2d)	0	h_g (shell-2d)	0	0.0
	5.0 ^g	t_{1u} (shell-2p*)	0	t_{1u} (shell-2p*)	0	
		t_{2g}	2	t_{2g}	2	
		h_g	5	h_g	5	
		t_{1g}	3	t_{1g}	3	
2	5.0	h_g (shell-2d)	0	h_g (shell-2d)	0	-0.014
		t_{1u} (shell-2p*)	1	t_{1u} (shell-2p*)	0	
		t_{2g}	3	t_{2g}	0	
		h_g	5	h_g	5	
		t_{1g}	3	t_{1g}	3	
3	5.0	h_g (shell-2d)	0	h_g (shell-2d)	0	-0.020
		t_{1u} (shell-2p*)	2	t_{1u} (shell-2p*)	0	
		t_{2g}	3	t_{2g}	0	
		h_g	5	h_g	4	
4	5.0	h_g (shell-2d)	0	h_g (shell-2d)	0	-0.029
	5.0 ^g	t_{1u} (shell-2p*)	3	t_{1u} (shell-2p*)	0	
		t_{2g}	3	t_{2g}	0	
		h_g	5	h_g	3	
5	5.0	a_g	0	a_g	0	+0.038
		h_g (shell-2d)	1	h_g (shell-2d)	0	
		t_{1u} (shell-2p*)	3	t_{1u} (shell-2p*)	0	
		t_{2g}	3	t_{2g}	0	
		h_g	5	h_g	2	
		t_{1g}	3	t_{1g}	3	

is almost independent of the spin configuration. The number of unpaired electrons is increased until the total energy becomes higher than that of the system having two fewer unpaired electrons. The spin configurations around the Fermi level and the total energies of LSDA and GGA are summarized in Table VI. The system with $S=3$ is the most stable in the Pt₁₃ cuboctahedron cluster. The difference by one total spin moment in the total energies of $S=0,1,2,3$ is less than 0.007 Hartree (0.19 eV) but that of $S=3$ and $S=4$ is 0.022 Hartree (0.60 eV).

The shell structure is shown in Fig. 3(a), and the components of each level are shown in Fig. 3(b). The atomic d -electron band is located in the energy range of -0.35 to -0.22 Hartree for the majority spin and -0.34 to -0.20 Hartree for the minority spin. The lowest level, denoted as a_{1g} in Fig. 3(a), corresponds to the $1s$ level of the shell structure, the next two, e_g and t_{2g} are the shell-1d levels, and the t_{1u} state at about -0.39 Hartree is the shell-1p level. Although the magnitude of DOS is small, the shell-2s also exists below the atomic d -band at about -0.37 a.u. of both the majority and minority spins. The bandwidth of the Pt₁₃ cuboctahedron cluster is very similar to that of the Pd₁₃ cuboctahedron cluster. For the shell structure below the d -band, $1s$, $1p$, and $2s$ exist in the Pt₁₃ cuboctahedron cluster, but $1s$ barely exists in the Pd₁₃ cuboctahedron cluster. The shell-

$2p^*$ of the Pt₁₃ cuboctahedron cluster is in the atomic d band at about -0.235 Hartree for the majority spin and at about -0.22 Hartree for the minority spin. The Fermi level is formed by the atomic d band in the Pt₁₃ cuboctahedron cluster. The total energy becomes higher when the t_{2g} state of the shell-2d is occupied, which corresponds to the $S=4$ system.

2. The Pt₁₃ icosahedron cluster

We analyzed the Pt₁₃ icosahedron cluster in the same way. The equilibrium spacing of the Pt₁₃ icosahedron clusters is 5.0 a.u., which is almost the same as that of the spin restricted result. The spin configurations around the Fermi level and the total energies of LSDA and GGA are summarized in Table VII. The system with $S=4$ is the most stable in the Pt₁₃ icosahedron cluster, which is one total spin moment larger than that of the Pt₁₃ cuboctahedron cluster. The total energy difference by one total spin moment of $S=0,1,2,3,4$ is less than 0.005 Hartree (0.14 eV) and the difference between $S=4$ and $S=5$ is 0.024 Hartree (0.65 eV). The shell structure of the $S=4$ system is shown in Fig. 4(a), and the components of each level are shown in Fig. 4(b). The atomic d -electron band is located in the energy range of -0.355 to -0.21 Hartree for the majority spin and -0.34 to

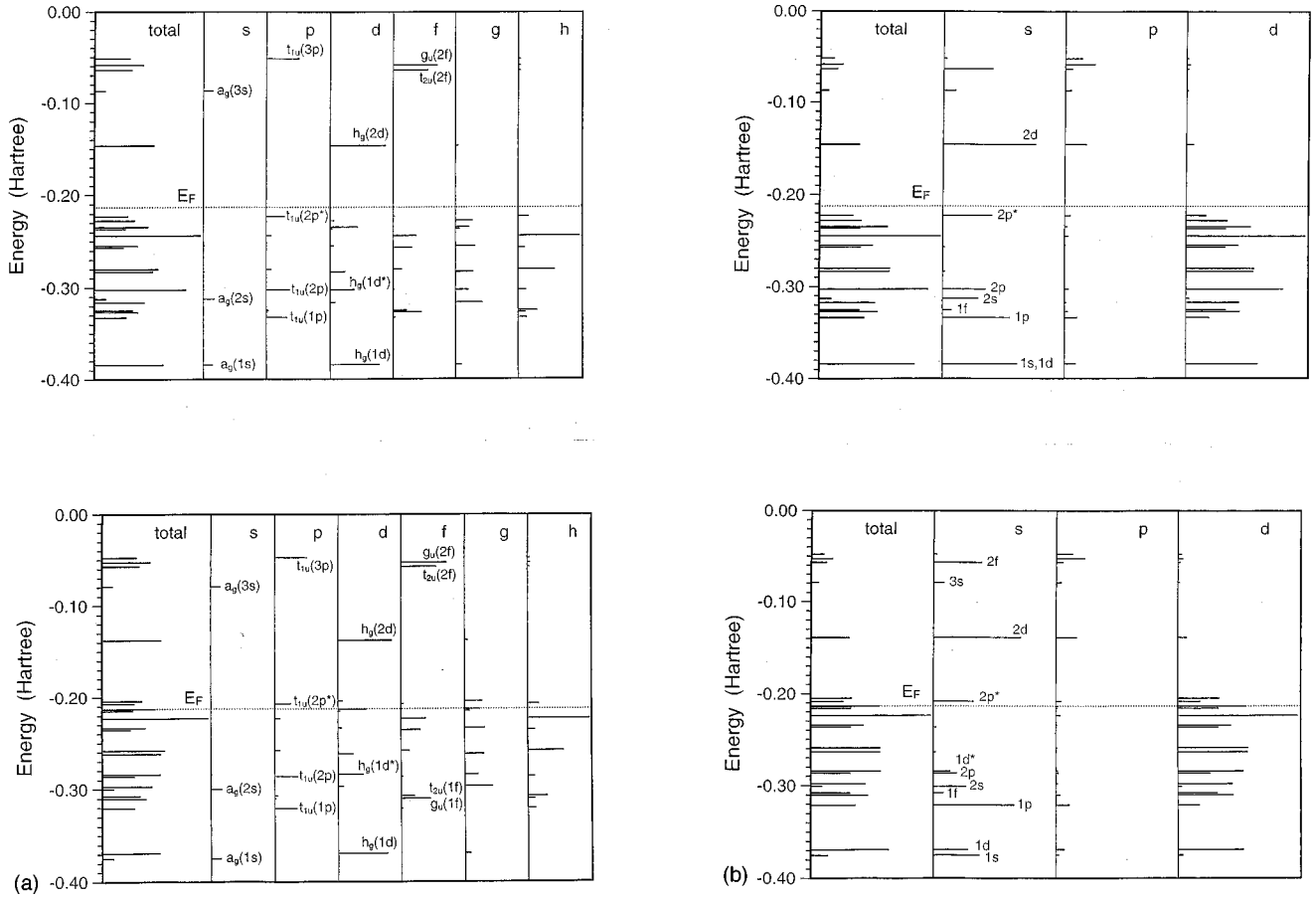


FIG. 2. (a) Energy levels and the density of states (DOS) of Pd₁₃ icosahedron cluster. *s*, *p*, *d*, *f*, *g*, and *h* indicate the partial DOS of each molecular orbital projected at the cluster center. R_{\max} for expansion is 15 Å. The upper figure is for the majority spin and the lower one is for the minority spin. (b) Same as (a) but augmented at 13 Pd atom sites with $R_{\max} = 1.6$ Å.

–0.19 Hartree for the minority spin, which is very similar to that in the cuboctahedron cluster. The lowest level, denoted as a_{1g} in Fig. 4(a), corresponds to the 1*s* level of the shell structure, the next one, h_g , is the shell-1*d* level, and the t_{1u} state at about –0.405 Hartree is the shell-1*p* level. Since the symmetry of an icosahedron is higher than that of a cuboctahedron, its shell structure is clearer. All the levels having a comparatively large atomic *s*-component can be consistently assigned to the shell structure shown in Fig. 4(b). The shell structure in the atomic *d*-band is thought to split into bonding and antibonding levels, as seen for the shell-1*d* or -2*p*. The Fermi level is formed by the atomic *d*-band in the Pt₁₃ icosahedron cluster. The total energy becomes higher when the h_g state of the shell-2*d* is occupied, which corresponds to the $S=5$ system. The difference between LDA and GGA potentials is negligible in the Pt₁₃ clusters.

D. Spin-orbit splitting

The nonlocal angular-momentum-dependent potential $\hat{V}_i^{\text{ion}}(r)$ is defined as an average pseudopotential of the different $j = l \pm \frac{1}{2}$ states, and the spin-orbit-interaction potential \hat{V}_i^{so} is given by the difference of the *j*-dependent potentials. Applying the pseudopotential parameters of Bachelet *et al.*,¹³ we can evaluate effects of the spin-orbit interaction on the states of Pd or Pt clusters using the following equations:

$$P_{vi,lm}(r_i) = \int \psi(\mathbf{r}_i) Y_{lm}(\mathbf{r}_i) d\Omega_i, \quad (8)$$

$$r_i \leq R_{\max}, \quad (9)$$

$$e_{vi,l} = \sum_m \int P_{vi,lm}(r) \hat{V}_l^{\text{so}}(r) P_{vi,lm}(r) r^2 dr, \quad (10)$$

$$\xi_{vi} = \sum_i e_{vi,l}, \quad (11)$$

where the subscript *i* indicates the atomic site on which the pseudopotential is located. R_{\max} is about 3 a.u.

Tables VIII and IX show the values of ξ_{vi} in Eq. (11) for the eigenstates of the Pd₁₃ and the Pt₁₃ cuboctahedron clusters around the Fermi level in the spin-restricted calculation. The average strength of spin-orbit splitting of the Pd₁₃ cluster is 0.007 Hartree, which is one-third of the value for the Pt₁₃ cluster, 0.02. The magnitude of the spin-orbit splitting of the shell states is smaller than this, 0.002 to 0.004 Hartree for Pd and 0.008 to 0.018 Hartree for Pt. Although the splitting energy is small, the LUMO and HOMO of Pd₁₃ could

TABLE VI. Spin configuration around Fermi level and total energy of Pt₁₃ cuboctahedron cluster. ΔE is the difference of total energy from the spin-restricted result of LSDA. Superscript ‘‘g’’ represents a value at equilibrium spacing of GGA. The other values are calculated at equilibrium spacing of LSDA.

S	Spacing (a.u.)	Spin configuration				ΔE by LSDA (Hartree)	ΔE by GGA (Hartree)
		Majority-spin		Minority-spin			
0	5.1	a_{2g}	0	a_{2g}	0	0.0	−0.001
	5.1 ^g	t_{1g}	1	t_{1g}	1		
		e_g	2	e_g	2		
1	5.1	a_{2g}	0	a_{2g}	0	−0.004	
		t_{1g}	2	t_{1g}	0		
		e_g	2	e_g	2		
		t_{1g}	3	t_{1g}	3		
2	5.1	a_{2g}	0	a_{2g}	0	−0.010	−0.013
		t_{1g}	3	t_{1g}	0		
		e_g	2	e_g	1		
		t_{1g}	3	t_{1g}	3		
3	5.1	t_{2g}	0	t_{2g}	0	−0.017	−0.027
	5.1 ^g	a_{2g}	1	a_{2g}	0		
		t_{1g}	3	t_{1g}	0		
		t_{2u}	3	t_{2u}	1		
		e_g	2	e_g	2		
4	5.1	t_{1g}	3	t_{1g}	3	+0.006	−0.004
		e_g	0	e_g	0		
		a_{1u}	0	a_{1u}	0		
		t_{2g}	1	t_{2g}	0		
		a_{2g}	1	a_{2g}	0		
		t_{1g}	3	t_{1g}	0		
		e_g	2	e_g	0		
t_{2u}	3	t_{2u}	2				
t_{1g}	3	t_{1g}	3				
t_{2g}	3	t_{2g}	3				

change places since the energy gap of the LUMO (shell- $2p^*$) and the HOMO of the Pd₁₃ cuboctahedron cluster is only 0.002 Hartree.

In Figs. 5(a) and 5(b) the diagrams of the spin-orbit splitting around the Fermi level are shown for the Pd₁₃ and Pt₁₃ cuboctahedron clusters. The splitting is analyzed in the one-electron approximation because of the Kohn-Sham scheme. Only the first-order perturbation of the orbital energy within its representation is taken into account. For the Pd cluster, the number of electrons on the left side of the diagram is 40, and they can consistently occupy up to the Γ_8 state at −0.2141 Hartree on the right side and form the closed orbital system again. The change in the total energy by the spin-orbit splitting is estimated to be −0.0122 Hartree, which shows the stabilization by the spin-orbit splitting. There are 34 electrons on the right side of the diagram for the Pt₁₃ cluster. When these electrons are put into the orbitals in the order of energy of the right side, the electrons occupy up to two states of Γ_8 at −0.2042 Hartree. The change in the total energy by the spin-orbit splitting is estimated to be −0.0820 Hartree.

Tables X and XI show the values of ξ_{vd} in Eq. (11) of the eigenstates for the Pd₁₃ and Pt₁₃ icosahedron clusters. Fig-

ures 6(a) and 6(b) are those diagrams considering the splitting by the symmetry around the Fermi level. The values of ξ_{vd} are similar to those of the cuboctahedron clusters but the widths of the split are larger due to the symmetry of the icosahedron. The change in the total energy by the spin-orbit splitting is estimated to be −0.0300 and −0.1082 Hartree for Pd and Pt, respectively. The icosahedron clusters gain more stabilization energy than the cuboctahedron clusters.

E. Jahn-Teller distortion

Since the Pd₁₃ icosahedron cluster and the Pt₁₃ clusters have an incompletely occupied HOMO, we need to consider the Jahn-Teller distortion. The Pd₁₃ cuboctahedron cluster also has unexpected degenerate orbitals at the HOMO according to the GGA calculation, which rouses our interest in the effect of the distortion. We calculated the force on the restricted orbital systems by the scheme explained in the Appendix. The Jahn-Teller theorem in the one-electron approximation requires the following splittings:

$$\begin{aligned}
 \text{Pd}_{13} \text{ icos: } T_{2g} \times T_{2g} &= T_{2g} + A_g + H_g, \\
 \text{Pt}_{13} \text{ icos: } T_{1g} \times T_{1g} &= T_{1g} + A_g + H_g, \\
 \text{Pt}_{13} \text{ fcc: } T_{1g} \times T_{1g} &= T_{1g} + T_{2g} + A_{1g} + E_g.
 \end{aligned}$$

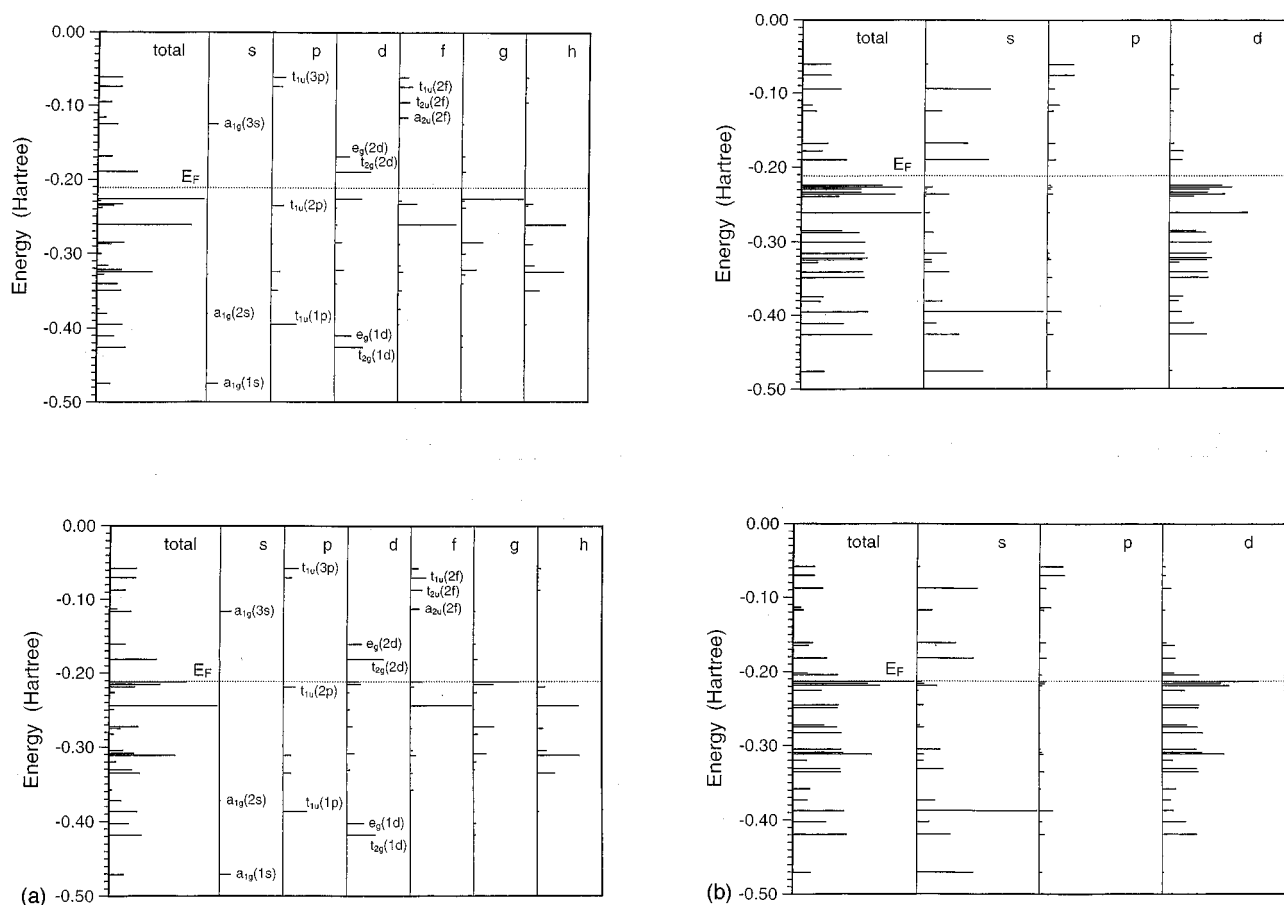


FIG. 3. (a) Energy levels and the density of states (DOS) of Pt_{13} cuboctahedron cluster. s , p , d , f , g , and h indicate the partial DOS of each molecular orbital projected at the cluster center. R_{max} for expansion is 15 Å. The upper figure is for the majority spin and the lower one is for the minority spin. (b) Same as (a) but augmented at 13 Pt atom sites with $R_{\text{max}} = 1.6$ Å.

Since the Pd_{13} cuboctahedron cluster has the closed HOMO, we did not estimate the Jahn-Teller effect. We have analyzed the force vectors by projecting to symmetrized atomic p -orbitals. The largest component belongs to H_g for the icosahedron clusters of both Pd and Pt metals. The Pt_{13} cuboctahedron cluster belongs to T_{2g} . We adopt these symmetrized force vectors as the distortion directions and minimize the total energy within the distortion in these directions. The distorted clusters are in C_{2h} and D_{4h} symmetries for the icosahedron clusters and the Pt_{13} cuboctahedron cluster, respectively. The total energy of the Pd_{13} icosahedron cluster is lowered 0.001 Hartree with 4% distortion of the cluster spacing, and that of the Pt_{13} icosahedron cluster is lowered 0.003 Hartree with 2% distortion of the cluster spacing. The Jahn-Teller distortion of the Pt_{13} icosahedron cluster is shown in Fig. 7. For the Pt_{13} cuboctahedron cluster, the total energy is lowered 0.001 Hartree with 0.4% distortion of the cluster spacing.

IV. DISCUSSION

The total energy and shell structure analysis shows that the spin configuration is related to the shell structure. The difference in the total energy of the different configuration for the atomic d -band state is smaller than about 0.005 Hartree, but that of the different configuration for the shell struc-

ture is more than 0.02 Hartree. The shell structure is occupied mainly by the atomic s electrons. The total energy becomes higher when the occupation changes across the energy gap of the shell structure. Unless the higher level of the shell structure is newly occupied, the higher spin state is more stable. That is, Hund's rule applies.

The configuration of the shell structure seems to be decided by the number of atomic s electrons. The Au_{13} cluster is well understood as the spherical jellium model of 13 atomic s -valence electrons,¹¹ which has five electrons in the shell- d state and which corresponds to the model with the region of the atomic d -band removed. The schematic energy level diagram for Pd_{13} , Pt_{13} , and Au_{13} is shown in Fig. 8, which removes the differences by the symmetry. In contrast to the Au_{13} cluster, the Pd_{13} cluster has no shell- $2d$ electron and partially has the shell- $2p$ electrons. The Pt_{13} cluster is comprehended as a system having five fewer shell-electrons than the Au_{13} cluster. The distinctive feature of the Pd_{13} cluster is the unoccupied shell- $2p^*$ state at just on the Fermi level. The Pd_{13} cluster seems to have a large s -electron affinity.

The effects of the GGA are not negligible, especially for the Pd_{13} clusters. The total energies are lowered about 0.01 Hartree and the higher spin polarization states become more stable, which is the opposite result of the LSDA. For the Pt

TABLE VII. Spin configuration around Fermi level and total energy of Pt₁₃ icosahedron cluster. ΔE is the difference of total energy from the spin restricted result of LSDA. Superscript ‘‘g’’ represents a value at equilibrium spacing of GGA. The other values are calculated at equilibrium spacing of LSDA.

S	Spacing (a.u.)	Spin configuration			ΔE by LSDA (Hartree)	ΔE by GGA (Hartree)
		Majority-spin		Minority-spin		
0	5.0	t_{2g}	0	t_{2g}	0	-0.001
	5.0 ^g	t_{1g}	2	t_{1g}	2	
		h_g	5	h_g	5	
1	5.0	t_{2g}	0	t_{2g}	0	-0.003
		t_{1g}	3	t_{1g}	1	
		h_g	5	h_g	5	
2	5.0	h_g (shell-2d)	0	h_g (shell-2d)	0	-0.002
		t_{2g}	1	t_{2g}	0	
		t_{1g}	3	t_{1g}	0	
		h_g	5	h_g	5	
3	5.0	h_g (shell-2d)	0	h_g (shell-2d)	0	-0.004
		t_{2g}	2	t_{2g}	0	
		t_{1g}	3	t_{1g}	0	
		h_g	5	h_g	4	
4	5.0	h_g (shell-2d)	0	h_g (shell-2d)	0	-0.009
		t_{2g}	3	t_{2g}	0	
		t_{1g}	3	t_{1g}	0	
		h_g	5	h_g	3	
5	5.0	a_g	0	a_g	0	+0.015
		h_g (shell-2d)	1	h_g (shell-2d)	0	
		t_{2g}	3	t_{2g}	0	
		t_{1g}	3	t_{1g}	0	
		h_g	5	h_g	2	
		t_{1u}	3	t_{1u}	3	

clusters, the effect of the GGA is not so serious. The changes in the total energy are ± 0.001 Hartree and the electronic structures are unchanged. The difference between Pd and Pt in the effect of the GGA is thought to result from their electronic structures. The Fermi level is located at the edge of the d band of the Pd clusters. Furthermore, there exists the shell- $2p$ state, therefore the total energies of the Pd clusters are inevitably sensitive to the exchange-correlation potential, which depends or does not depend on the derivative of the charge density. On the other hand, the Fermi level of the Pt clusters is located in the d band. A little change of the location of the Fermi level does not change the derivative of the charge density and the converse will hold.

The effect of the spin polarization (ΔE^{sp}) is 0.01–0.035 Hartree. The effects of the spin-orbit splitting (ΔE^{so}) are 0.01–0.03 Hartree for the Pd clusters, and 0.08–0.1 Hartree for the Pt clusters. The spin-orbit splitting depends on the cluster symmetry and the stabilization of the icosahedron cluster is larger than that of the cuboctahedron one. The Jahn-Teller effect (ΔE^{JT}) is small, the change in the total energy is the order of 0.001 Hartree. The higher symmetry seems to be favorable in the microclusters of 13 atoms to

keep their electronic shell structures. Taking all these effects into account, the stable structures of Pd₁₃ and Pt₁₃ clusters are predicted as follows:

$$\Delta E_{\text{tot}} \equiv [E_{\text{tot}}^{\text{GGA}}(\text{icos}) + \Delta E^{\text{so}}(\text{icos}) + \Delta E^{\text{sp}}(\text{icos}) + \Delta E^{\text{JT}}(\text{icos})] - [E_{\text{tot}}^{\text{GGA}}(\text{fcc}) + \Delta E^{\text{so}}(\text{fcc}) + \Delta E^{\text{sp}}(\text{fcc}) + \Delta E^{\text{JT}}(\text{fcc})], \quad (12)$$

$$\Delta E_{\text{tot}}(\text{Pd}) = (-376.540 - 0.030 - 0.034 - 0.001) - (-376.588 - 0.012 - 0.015) = +0.010, \quad (13)$$

$$\Delta E_{\text{tot}}(\text{Pt}) = (-341.752 - 0.108 - 0.010 - 0.003) - (-341.803 - 0.082 - 0.026 - 0.001) = +0.039. \quad (14)$$

For both Pd and Pt metals the cuboctahedron clusters are more stable.

For the Pd₁₃ clusters we found two relevant works comparing with our results. One is that of Reddy *et al.* using a

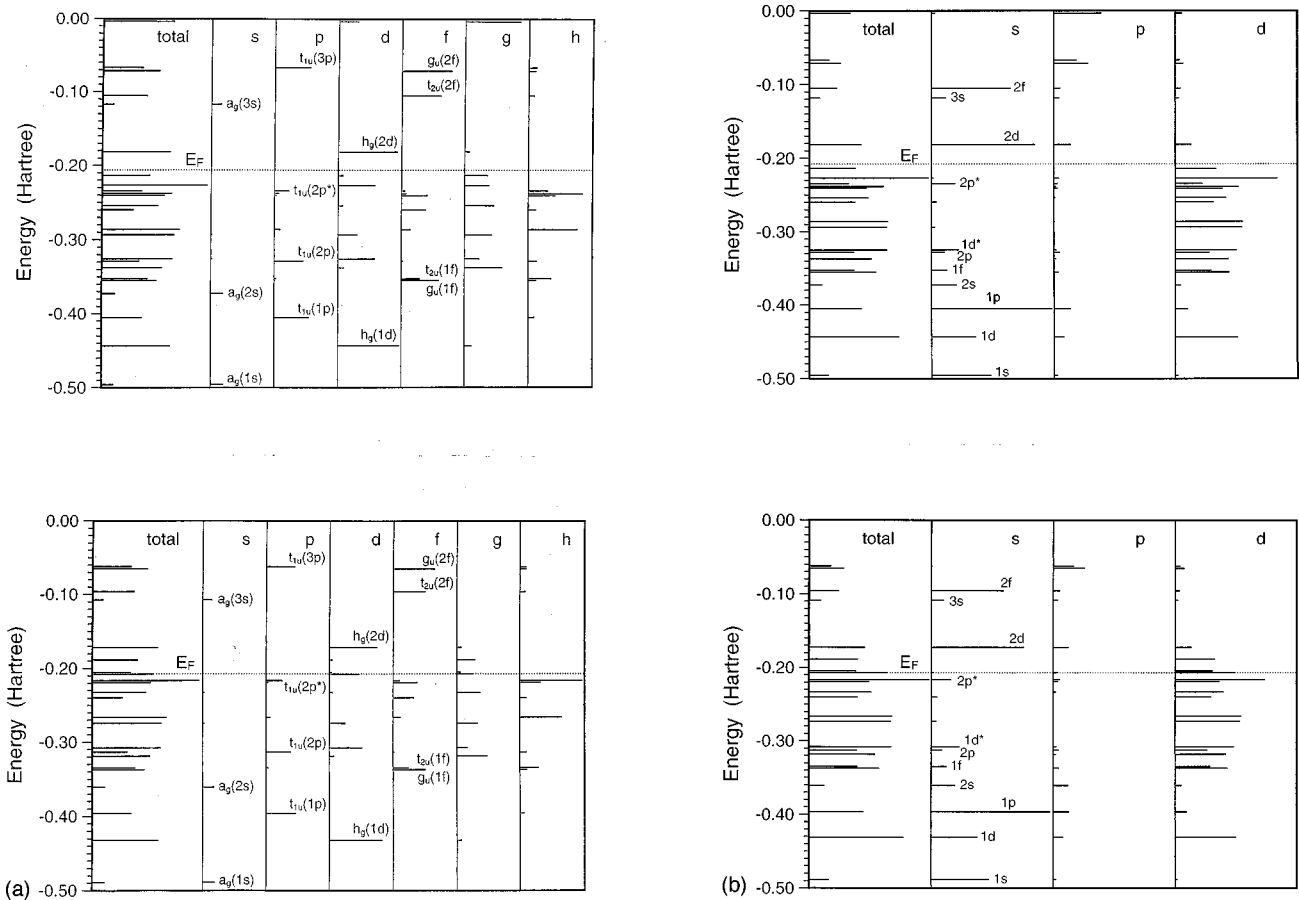


FIG. 4. (a) Energy levels and the density of states (DOS) of Pt_{13} icosahedron cluster. s , p , d , f , g , and h indicate the partial DOS of each molecular orbital projected at the cluster center. R_{max} for expansion is 15 Å. The upper figure is for the majority spin and the lower one is for the minority spin. (b) Same as (a) but augmented at 13 Pt atom sites with $R_{\text{max}} = 1.6$ Å.

density-functional scheme with the discrete variational method (DVM) with numerical bases or a Gaussian basis.² The spin-polarized icosahedron cluster is the most stable. The difference between the icosahedron cluster and the cuboctahedron cluster in the total energy is $\Delta E(\text{icos-fcc}) = -0.018$ Hartree. Another is that of Estiú *et al.* with the intermediate neglect of differential overlap (INDO) model at

the self-consistent-field-configuration-interaction (SCF-CI) level.³ The triplet icosahedron cluster is the most stable and this cluster is to be distorted by the Jahn-Teller effect. The distortion vector belongs to the H_g representation, which is the same as our result. The difference between the icosahedron and cuboctahedron clusters in the total energy is $\Delta E(\text{icos-fcc}) = -0.067$ Hartree.

The total energy of the cuboctahedron cluster is lower than that of the icosahedron cluster only in our result

TABLE VIII. Estimate of the spin-orbit interaction strength ξ_{vd} around the Fermi level for the Pd_{13} cuboctahedron cluster.

Representation	Energy (Hartree)	ξ_{vd}
t_{2g} (shell-2d)	-0.145 740	0.001 762
a_{1u}	-0.184 570	0.008 264
t_{1u} (LUMO, shell-2p)	-0.207 640	0.004 265
e_g (HOMO)	-0.212 900	0.007 688
t_{2g}	-0.213 110	0.007 292
a_{2g}	-0.214 090	0.007 602
t_{1g}	-0.214 140	0.007 628
t_{2u}	-0.218 090	0.007 247
t_{1g}	-0.218 360	0.007 183
e_u	-0.221 810	0.007 401
t_{2u}	-0.223 440	0.007 463

TABLE IX. Estimation of the spin-orbit interaction strength ξ_{vd} around the Fermi level for the Pt_{13} cuboctahedron cluster.

Representation	Energy (Hartree)	ξ_{vd}
a_{1u}	-0.172 380	0.024 787
t_{2g} (shell-2d)	-0.185 680	0.013 892
a_{2g} (LUMO)	-0.214 400	0.022 928
t_{1g} (HOMO)	-0.215 890	0.023 329
e_g	-0.220 130	0.023 426
t_{1g}	-0.221 410	0.022 843
t_{2g}	-0.222 340	0.022 547
t_{2u}	-0.222 660	0.021 493
e_u	-0.226 880	0.022 710
t_{2u}	-0.226 920	0.021 950

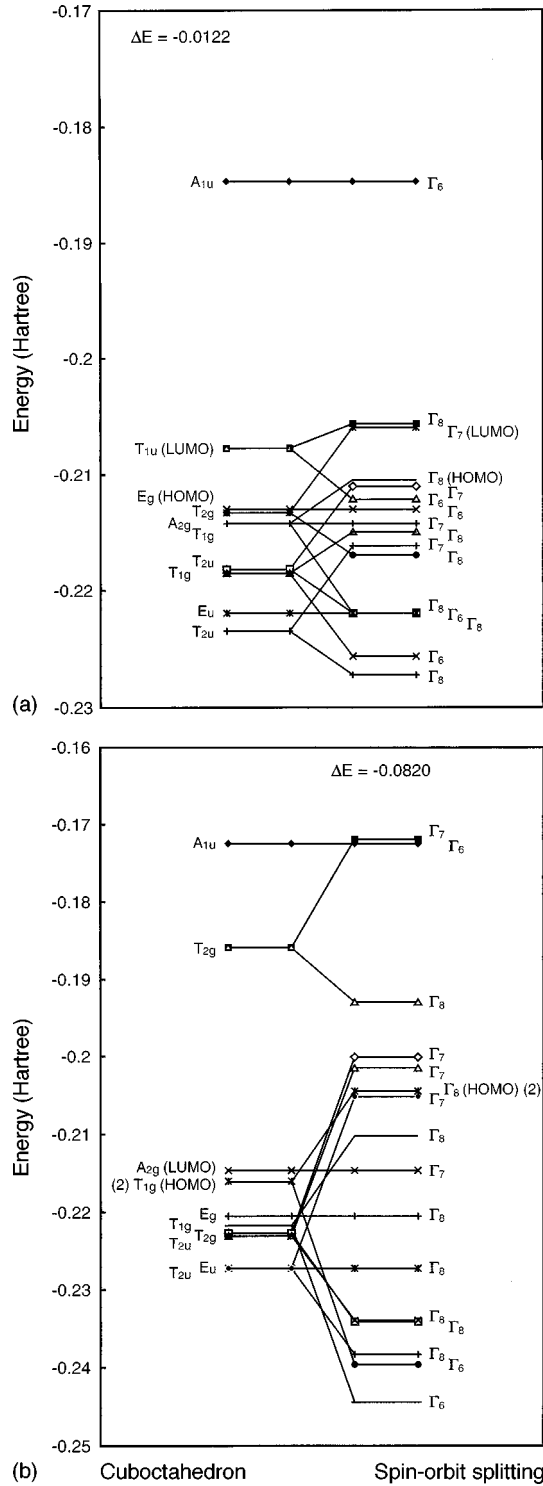


FIG. 5. (a) The diagram of spin-orbit splitting of HOMO and LUMO of Pd₁₃ cuboctahedron cluster. (b) The diagram of spin-orbit splitting of HOMO and LUMO of Pt₁₃ cuboctahedron cluster.

[$\Delta E(\text{icos-fcc}) = 0.048$ Hartree with the GGA]. The two results except ours show that the $S=0$ state of A_{1g} is the most stable in the cuboctahedron symmetry. For the icosahedron cluster of the $S=0$ state, the ordering of the frontier molecular orbitals in our result is almost the same as in Estiú's result but for the position of the a_{1g} state corresponding to

TABLE X. Estimation of spin-orbit interaction strength ξ_{vd} around the Fermi level for the Pd₁₃ icosahedron cluster.

Representation	Energy (Hartree)	ξ_{vd}
t_{1u} (LUMO, shell-2p)	-0.207 720	0.004 330
t_{2g} (HOMO)	-0.208 730	0.007 855
h_g	-0.211 310	0.007 525
t_{1g}	-0.217 600	0.007 585
h_u	-0.224 950	0.007 335
g_u	-0.225 160	0.007 081

the shell-3s state. In the icosahedron cluster, the higher S state is more stable (until the shell-2d state is occupied) in Reddy's and our calculations. The crucial difference between our result and the other two results is that the cuboctahedron cluster is stabler than the icosahedron cluster for Pd. This might be due to the accuracy of the numerical calculation and the treatment of the core electrons.

The present calculations were done on an NEC supercomputer SX-4 system (8 CPU's with 16 Gbyte memory). The program codes were fully parallelized for the number of atomic sites. The time-consuming calculations of GGA and the forces were efficiently processed.

APPENDIX

In the present LCPSAO scheme with the nonlocal pseudo-potential term, the gradient force is represented by three main terms, the Hellmann-Feynman force \mathbf{F}_i^{HF} , the basis-set correction term \mathbf{F}_i^{BS} , and the density-basis correction term \mathbf{F}_i^{DB} . The main part for this force calculation is that of the nonlocal potential part,

$$\mathbf{F}_i = - \frac{\partial E_H}{\partial \mathbf{R}_i} = \mathbf{F}_i^{\text{HF}} + \mathbf{F}_i^{\text{BS}} + \mathbf{F}_i^{\text{DB}}, \quad (\text{A1})$$

$$\mathbf{F}_i^{\text{HF}} = - \sum_{\nu} f_{\nu} \left\langle \psi_{\nu} \left| \frac{\partial \tilde{H}}{\partial \mathbf{R}_i} \right| \psi_{\nu} \right\rangle_{\rho} - \frac{\partial E_{\text{NN}}}{\partial \mathbf{R}_i}, \quad (\text{A2})$$

TABLE XI. Estimation of spin-orbit interaction strength ξ_{vd} around the Fermi level for the Pt₁₃ icosahedron cluster.

Representation	Energy (Hartree)	ξ_{vd}
h_g (shell-2d)	-0.176 890	0.013 925
t_{2g} (LUMO)	-0.207 900	0.023 549
t_{1g} (HOMO)	-0.217 770	0.023 142
h_g	-0.218 310	0.023 328
t_{1u}	-0.226 810	0.018 509
h_u	-0.229 990	0.022 338
g_u	-0.235 260	0.021 883
g_g	-0.245 330	0.021 296
t_{2u}	-0.247 850	0.020 863

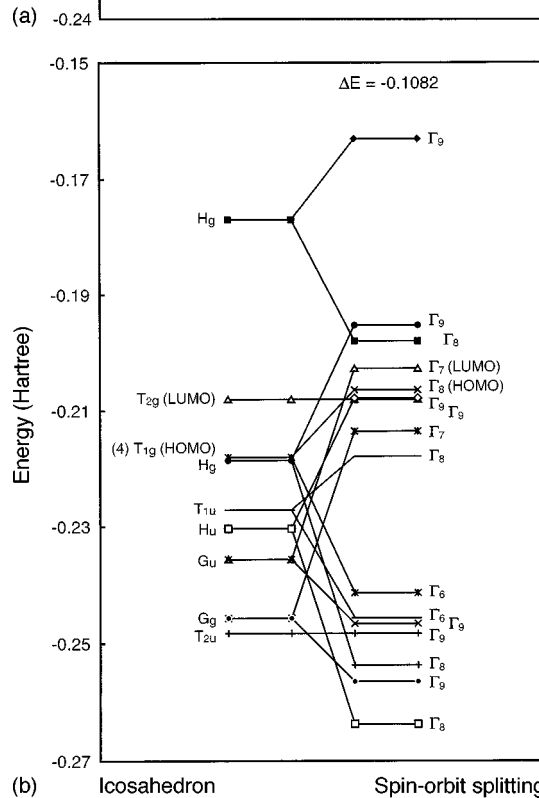
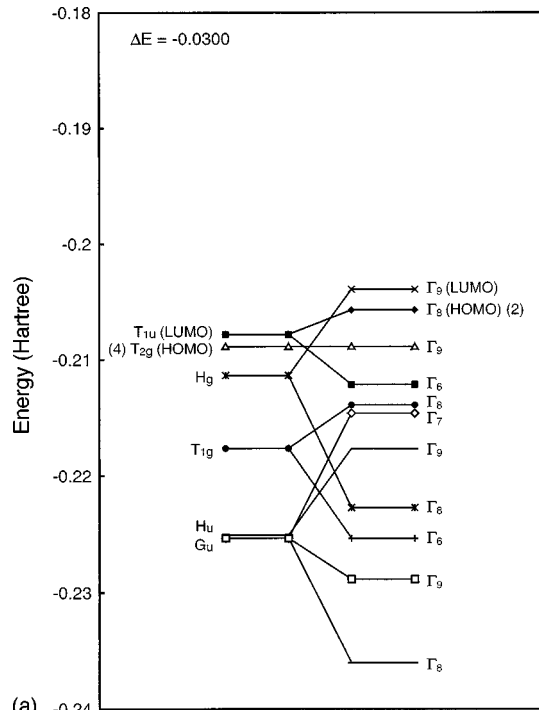


FIG. 6. (a) The diagram of spin-orbit splitting of HOMO and LUMO of Pd_{13} icosahedron cluster. (b) The diagram of spin-orbit splitting of HOMO and LUMO of Pt_{13} icosahedron cluster.

$$\mathbf{F}_i^{\text{BS}} = - \sum_{\nu} f_{\nu} \int \frac{\partial \psi_{\nu}^*(\mathbf{r})}{\partial \mathbf{R}_i} \tilde{H} \psi_{\nu}(\mathbf{r}) d\mathbf{r} + \text{c.c.}, \quad (\text{A3})$$

$$\mathbf{F}_i^{\text{DB}} = \int \delta \rho(\mathbf{r}) \left[\frac{\partial \tilde{\phi}(\mathbf{r})}{\partial \mathbf{R}_i} + \frac{\partial \tilde{\rho}(\mathbf{r})}{\partial \mathbf{R}_i} \frac{dV_{\text{XC}}(\tilde{\rho})}{d\tilde{\rho}} \right] d\mathbf{r}. \quad (\text{A4})$$

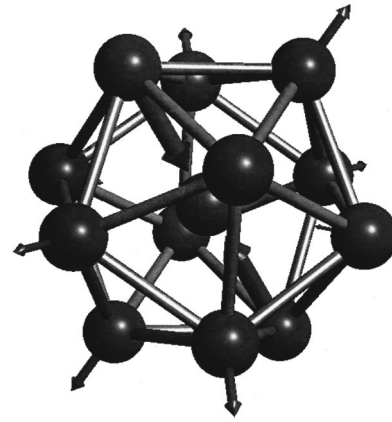


FIG. 7. The Jahn-Teller distortion of the Pt_{13} icosahedron cluster. The length and thickness of the distortion arrow are in proportion to the magnitude of the distortion vector.

\mathbf{F}^{HF} in Eq. (A2) is given by the derivative of potential energies explicitly dependent on \mathbf{R}_i by fixing $\tilde{\rho}$. Averill-Painter's density-basis correction term \mathbf{F}^{DB} comes from the \mathbf{R}_i dependence, where $\tilde{\rho}$ represents the input charge density and ρ represents the output charge density of the SCF calculation. When good convergence is attained in the SCF, this density-basis correction term is negligible.

Computational details are as follows. The first term in \mathbf{F}^{HF} is given by

$$\frac{\partial E_{\text{NN}}}{\partial x_i} = - \sum_{i \neq j} \frac{Z_i Z_j}{|\mathbf{R}_i - \mathbf{R}_j|} \frac{(x_i - x_j)}{|\mathbf{R}_i - \mathbf{R}_j|}, \quad (\text{A5})$$

where $\mathbf{R}_i = (x_i, y_i, z_i)$.

The nonlocal pseudopotential term is given by the direct numerical differentials of Richardson's extrapolations and the contribution from the V_{core} term is given analytically,

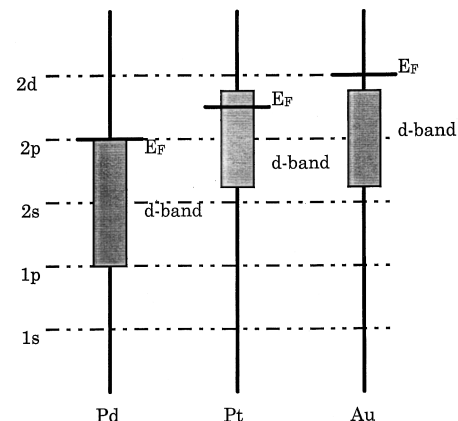


FIG. 8. The schematic energy level diagram for Pd_{13} , Pt_{13} , and Au_{13} .

$$\frac{\partial \hat{V}_l^{\text{ion}}(\mathbf{r})}{\partial x_i} = \frac{\partial \hat{V}_l^{\text{ion}}(\mathbf{r}-\mathbf{R}_i)}{\partial x_i} = \left\{ 4 \times \frac{\hat{V}_l^{\text{ion}}(\mathbf{r}-\mathbf{R}_i-2\Delta x) - \hat{V}_l^{\text{ion}}(\mathbf{r}-\mathbf{R}_i+2\Delta x)}{4\Delta x} - \frac{\hat{V}_l^{\text{ion}}(\mathbf{r}-\mathbf{R}_i-\Delta x) - \hat{V}_l^{\text{ion}}(\mathbf{r}-\mathbf{R}_i+\Delta x)}{2\Delta x} \right\} / 3. \quad (\text{A6})$$

Δx is a minute value for x, y, z directions. The effect of Richardson's extrapolation is $\mathcal{O}(10^{-3})$.

The basis-set correction term \mathbf{F}^{BS} is also calculated numerically,²⁰

$$F_{i,x}^{\text{BS}} = \left\langle \frac{\partial \psi_v}{\partial x_i} \left| \tilde{H} \right| \psi_v \right\rangle + \text{c.c.} \quad (\text{A7})$$

$$= \left\{ \int \left[\sum_{jlm, j \neq i} c_{jlm}^v \chi_{jlm} \right. \right. \\ \left. \left. + \sum_{ilm} c_{ilm}^v \chi_{ilm}(\mathbf{r}-\mathbf{R}_i-\Delta x) \right] \tilde{H} \psi_v d\mathbf{r} - \int \left[\sum_{jlm, j \neq i} c_{jlm}^v \chi_{jlm} \right. \right. \\ \left. \left. + \sum_{ilm} c_{ilm}^v \chi_{ilm}(\mathbf{r}-\mathbf{R}_i+\Delta x) \right] \tilde{H} \psi_v d\mathbf{r} \right\} / 2\Delta x + \text{c.c.}, \quad (\text{A8})$$

$$\psi_v \equiv \sum_{jlm} c_{jlm}^v \chi_{jlm},$$

where the kinetic energy part is evaluated by

$$-\frac{1}{2} \nabla^2 \chi_{jlm} = [\epsilon_{\text{atom}}^l - V_{\text{val}}^{\text{atom}}(r) - \hat{V}_N(r)] \chi_{jlm}. \quad (\text{A9})$$

-
- ¹B. I. Dunlap, Phys. Rev. A **41**, 5691 (1990).
²B. V. Reddy, S. N. Khanna, and B. I. Dunlap, Phys. Rev. Lett. **70**, 3323 (1993).
³G. L. Estiú and M. C. Zerner, J. Phys. Chem. **98**, 4793 (1994).
⁴J. Zhao, X. Chen, Q. Sun, F. Liu, and G. Wang, Europhys. Lett. **32**, 113 (1995).
⁵D. C. Douglass, J. P. Bucher, and L. A. Bloomfield, Phys. Rev. B **45**, 6341 (1992).
⁶A. J. Cox, J. G. Louderback, S. E. Apsel, and L. A. Bloomfield, Phys. Rev. B **49**, 12 295 (1994).
⁷S. E. Apsel, J. W. Emmert, J. Deng, and L. A. Bloomfield, Phys. Rev. Lett. **76**, 1441 (1996).
⁸N. Watari and S. Ohnishi, J. Phys. Chem. **106**, 7531 (1997).
⁹N. Fujima and T. Yamaguchi, J. Phys. Soc. Jpn. **58**, 1334 (1989).
¹⁰N. Fujima and T. Yamaguchi, J. Phys. Soc. Jpn. **58**, 3290 (1989).
¹¹N. Watari and S. Ohnishi (unpublished).
¹²S. A. Stanislaus and B. H. Cooper, Catal. Rev. Sci. Eng. **36**, 75 (1994).
¹³G. B. Bachelet, D. R. Hamann, and M. Schluter, Phys. Rev. B **26**, 4199 (1982).
¹⁴S. Ohnishi and N. Watari, Phys. Rev. B **49**, 14 619 (1994).
¹⁵N. Watari and S. Ohnishi, Catal. Today **23**, 371 (1995).
¹⁶J. P. Perdew and A. Zunger, Phys. Rev. B **23**, 5048 (1981).
¹⁷J. P. Perdew, K. Burke, and M. Ernzerhof, Phys. Rev. Lett. **77**, 3865 (1996).
¹⁸A. D. Becke, J. Phys. Chem. **88**, 2547 (1988).
¹⁹Y. Ishii (unpublished); see also Y. Ishii, S. Ohnishi, and S. Sugano, Phys. Rev. B **33**, 5271 (1986).
²⁰F. W. Averill and G. S. Painter, Phys. Rev. B **41**, 10 344 (1990).